

Communication

Enhanced Magnetocaloric Properties of Annealed Melt-Extracted $\text{Mn}_{1.3}\text{Fe}_{0.6}\text{P}_{0.5}\text{Si}_{0.5}$ Microwires

Lin Luo^{1,2}, Jia Yan Law^{2,*} , Hongxian Shen¹ , Luis M. Moreno-Ramírez² , Victorino Franco² , Shu Guo¹, Nguyen Thi My Duc^{3,4} , Jianfei Sun^{1,*} and Manh-Huong Phan^{3,*}¹ School of Materials Science and Engineering, Harbin Institute of Technology, Harbin 150001, China² Department of Condensed Matter Physics, University of Seville, 41080 Seville, Spain³ Department of Physics, University of South Florida, Tampa, FL 33620, USA⁴ Department of Material Science, Faculty of Physics, The University of Danang—University of Science and Education, 459 Ton Duc Thang, Lien Chieu, Danang 550000, Vietnam

* Correspondence: jylaw@us.es (J.Y.L.); jfsun@hit.edu.cn (J.S.); phanm@usf.edu (M.-H.P.)

Abstract: The highly regarded Fe_2P -based magnetocaloric materials are usually fabricated by ball milling, and require an additional extended annealing treatment at high temperatures (at temperatures up to 1423 K for several hours to days). In this work, we show that fabricating $\text{Mn}_{1.3}\text{Fe}_{0.6}\text{P}_{0.5}\text{Si}_{0.5}$ into the form of microwires attained 82.1 wt.% of the desired Fe_2P phase in the as-cast state. The microwires show a variable solidification structure along the radial direction; close to the copper wheel contact, Fe_2P phase is in fine grains, followed by dendritic Fe_2P grains and finally secondary $(\text{Mn,Fe})_5\text{Si}_3$ phase in addition to the dendritic Fe_2P grains. The as-cast microwires undergo a ferro- to para-magnetic transition with a Curie temperature of 138 K, showing a maximum isothermal magnetic entropy change of $4.6 \text{ J kg}^{-1} \text{ K}^{-1}$ for a magnetic field change of 5 T. With further annealing, a two-fold increase in the maximum isothermal magnetic entropy change is found in the annealed microwires, which reveal 88.1 wt.% of Fe_2P phase.

Keywords: melt-extraction technique; $(\text{Mn,Fe})_2(\text{P,Si})$ microwires; microstructure; magnetocaloric effect



Citation: Luo, L.; Law, J.Y.; Shen, H.; Moreno-Ramírez, L.M.; Franco, V.; Guo, S.; Duc, N.T.M.; Sun, J.; Phan, M.-H. Enhanced Magnetocaloric Properties of Annealed Melt-Extracted $\text{Mn}_{1.3}\text{Fe}_{0.6}\text{P}_{0.5}\text{Si}_{0.5}$ Microwires. *Metals* **2022**, *12*, 1536. <https://doi.org/10.3390/met12091536>

Academic Editor: Volodymyr A. Chernenko

Received: 30 July 2022

Accepted: 13 September 2022

Published: 16 September 2022

Publisher's Note: MDPI stays neutral with regard to jurisdictional claims in published maps and institutional affiliations.



Copyright: © 2022 by the authors. Licensee MDPI, Basel, Switzerland. This article is an open access article distributed under the terms and conditions of the Creative Commons Attribution (CC BY) license (<https://creativecommons.org/licenses/by/4.0/>).

1. Introduction

Solid-state magnetic refrigeration is considered a potential alternative to the conventional vapor-compression techniques due to its high energy efficiency and environmental friendliness [1–6]. The development of magnetic refrigerators depends on the performance of magnetic refrigerants, those having significant magnetocaloric effect (MCE) [7–9]. $(\text{Mn,Fe})_2(\text{P,Si})$ materials are one of the most promising magnetic refrigerants due to their high magnetocaloric performance, relatively low hysteresis and abundance of the raw materials [10–12].

Regarding the synthesis procedures, it is noticeable that most of the reported $(\text{Mn,Fe})_2(\text{P,Si})$ systems are prepared by ball milling and/or arc melting methods [13,14]. However, these methods usually require time-consuming heat treatment (from several hours to several days) for achieving homogeneous compositions and forming high fractions of the Fe_2P phase [9]. Alternatively, rapid solidification techniques, such as melt spinning [15,16] and droplet melting [17,18], enable the fabrication of materials with excellent compositional homogeneity and reduced impurities after short-time heat treatment. In this way, melt-extraction as a rapid solidification technique has been proposed as a promising method to develop wire-shaped magnetocaloric materials as reported for melt-extracted Gd-based microwires [19,20] and more recently high-entropy alloys [21,22], as well as medium-entropy alloys [23]. Moreover, theoretical calculations suggest that wire-shaped magnetic refrigerants with high packing factors could result in a larger working frequency compared to particles and layers [24,25]. Their micro-size diameters could improve the heat transfer of the cooling system [24]. Hence, it will be of interest to study

(Mn,Fe)₂(P,Si) melt-extraction microwires and their structural and magnetocaloric behavior. The as-cast microwires show a variable solidification structure for the Fe₂P phase going from fine to dendritic grains along the radial direction. An elevated amount (82.1 wt.%) of the desired Fe₂P phase is obtained in the as-cast Mn_{1.3}Fe_{0.6}P_{0.5}Si_{0.5} microwires, which gives an isothermal magnetic entropy change peak value of 4.6 J kg⁻¹ K⁻¹ (for 5 T) at 145 K. A two-fold increase to 10.5 J kg⁻¹ K⁻¹ is achieved with further annealing at 1373 K for 15 min.

2. Materials and Methods

The MCE of (Mn,Fe)₂(P,Si) can be tuned by varying the Fe and Si content [26–28]. We have selected $x = 0.6$ in Mn_{2-x}Fe_xSi_{0.5}P_{0.5} due to the minimized hysteresis reported in ref. [27]. In addition, for this family of compounds, slight deficiency in transition metal elements can reduce the impurities and thermal hysteresis [29,30]. Therefore, the composition of Mn_{1.3}Fe_{0.6}P_{0.5}Si_{0.5} was chosen for researching. An ingot was prepared by arc-melting in argon atmosphere from a mixture of raw materials: Mn (99.5%), P (99.5%), FeP chunks (98%) and Si (99.999%). For accounting for the loss of Mn during arc-melting, an excess of 5 wt.% of Mn was added to the mixture. The ingot was re-melted at least six times with electromagnetic stirring then suction casted into an 8 mm diameter rod for subsequent melt-extraction into microwires. Using a melt feeding speed of 20 μm/s and a 30 cm diameter Cu wheel with a linear speed of 30 m/s, up to 7 cm long as-cast microwires with ~35 μm diameters were obtained. For annealing studies, the microwires were sealed in a quartz tube under Ar atmosphere and annealed at 1373 K for 15 min and then water quenched.

The measurements were performed, employing a large quantity from the as-cast and annealed microwires, giving that the obtained results are the average from the studied samples. Powder X-ray diffraction (XRD) experiments at room temperature using Cu-K_α radiation were performed to characterize for the crystal structure and phase composition of the microwires. Microstructural and compositional details were obtained on a field emission scanning electron microscope (SIGMA-500-Zeiss) with an energy dispersive spectrometer (EDS). Magnetic measurements were carried out on a Quantum Design Physical Property Measurement System (PPMS-16 T) using a standard vibrating sample magnetometer (VSM) option. A set of the microwire arrays were close packed in a sample holder with a length of ~3 mm and an inner diameter of ~1 mm. To avoid virgin effects, the samples were precooled down to 10 K. Isothermal magnetization measurements were performed using a discontinuous protocol for erasing the magnetic hysteresis prior to any measurement [31]. The isothermal magnetic entropy change (ΔS_{iso}) is indirectly determined from magnetization measurements by applying the Maxwell relation:

$$\Delta S_{iso} = \mu_0 \int_0^H \left(\frac{\partial M}{\partial T} \right)_{H'} dH' \quad (1)$$

The relative cooling power (RCP) are calculated using the following Equation:

$$RCP = \Delta S_{iso}^{pk} \delta_{FWHM}, \quad (2)$$

where (δ_{FWHM}) is the full width at half maximum of the peak of isothermal magnetic entropy change (ΔS_{iso}^{pk}).

3. Results and Discussion

The XRD patterns of the as-cast microwires and the Rietveld refinement results show a main phase (82.1(7) wt.%) of the desired Fe₂P hexagonal structure (space group of $P\bar{6}2m$) in addition to minority (Mn,Fe)₅Si₃ phase (space group of $P6_3/mcm$) as displayed in Figure 1a. As this Fe₂P phase contributes to the giant MCE of the Mn-Fe-P-Si family, it is worth highlighting for its phase amount obtained in the as-cast microwires since its

enhancement usually requires annealing of the as-cast ingots as reported in ref. [12]. The lattice parameters found for the Fe_2P phase are $a = b = 6.09513(13) \text{ \AA}$, $c = 3.45230(10) \text{ \AA}$.

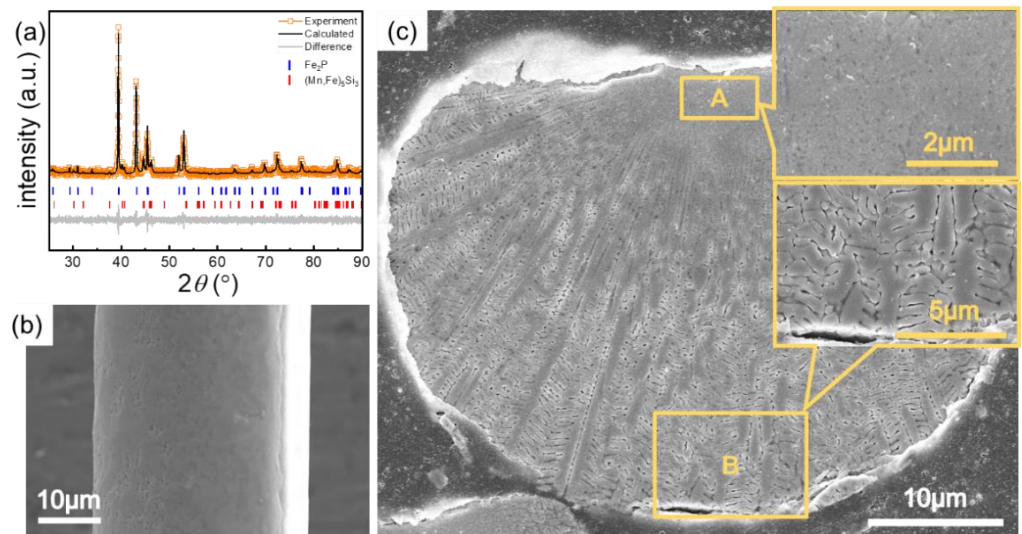


Figure 1. (a) XRD and Rietveld refinement results of the as-cast microwires. SEM of the (b) surface and (c) radial cross-section of the as-cast microwires.

The as-cast microwires are observed with a continuous and smooth surface as evidenced from their scanning electron micrograph (SEM) presented in Figure 1b. Further etching them with 4 wt.% hydrofluoric acid for 3 min, the radial cross-section of the microwires in Figure 1c reveals groove defects at the Cu-wheel side. Further magnification shows fine equiaxed grains near the wheel contact (see area A), while fine dendrites are observed (area B) further away from the wheel contact zone.

The EDS maps of the axial cross-section of the microwires presented in Figure 2a reveal an overall uniform element distribution. Only very minor fluctuations for P and Si concentrations are noticed along the radial directions when performing EDS line scans across the width and cross-section of the microwires (Figure 2b,c). These local inhomogeneities could be attributed to the existence of impurity $(\text{Mn,Fe})_5\text{Si}_3$ phase previously observed from XRD data.

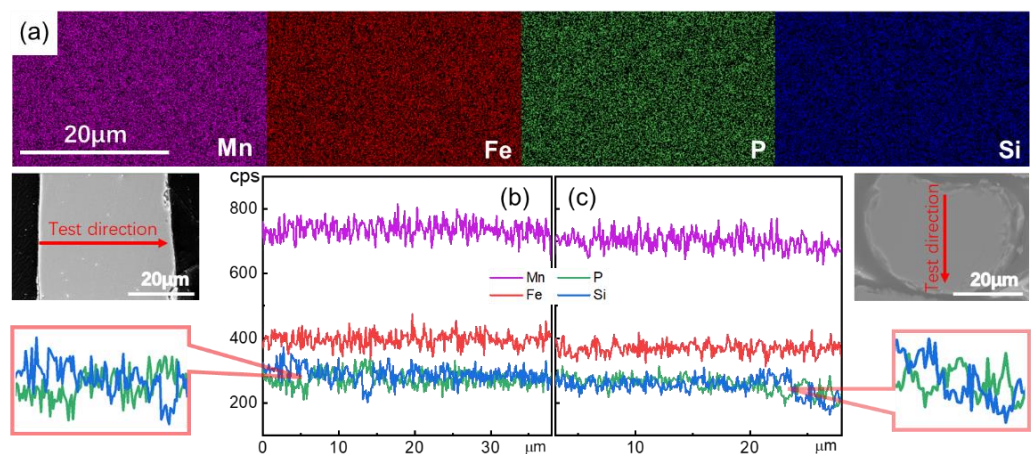


Figure 2. (a) EDS maps of axial cross-section of the as-cast microwire. EDS line scans (b) along the width of the microwire and (c) the microwire cross-section.

Figure 3a presents the $M(T)$ data of the as-cast microwires for 0.05 T and their derivatives in the inset, showing the Curie temperature (T_C) of 138 K. The magnetization and

specific heat measurements [32,33] are common methods for calculating the MCE performance of the materials. Here, isothermal magnetization curves were measured for determining the isothermal magnetic entropy change. Figure 3b presents the isothermal magnetic entropy change as a function of temperature for magnetic field change up to 5 T. Their peak values ($\Delta S_{\text{iso}}^{\text{pk}}$) for a field change of 2 and 5 T are found to be 1.9 and 4.6 $\text{J kg}^{-1} \text{K}^{-1}$, respectively. The temperature corresponding to $\Delta S_{\text{iso}}^{\text{pk}}$ values, denoted as T_{pk} , is around 145 K. Furthermore, it has to be noted that despite the elevated content of the Fe_2P phase, the existence of the $(\text{Mn,Fe})_5\text{Si}_3$ impurity phase could have a detrimental effect on the magnetocaloric properties.

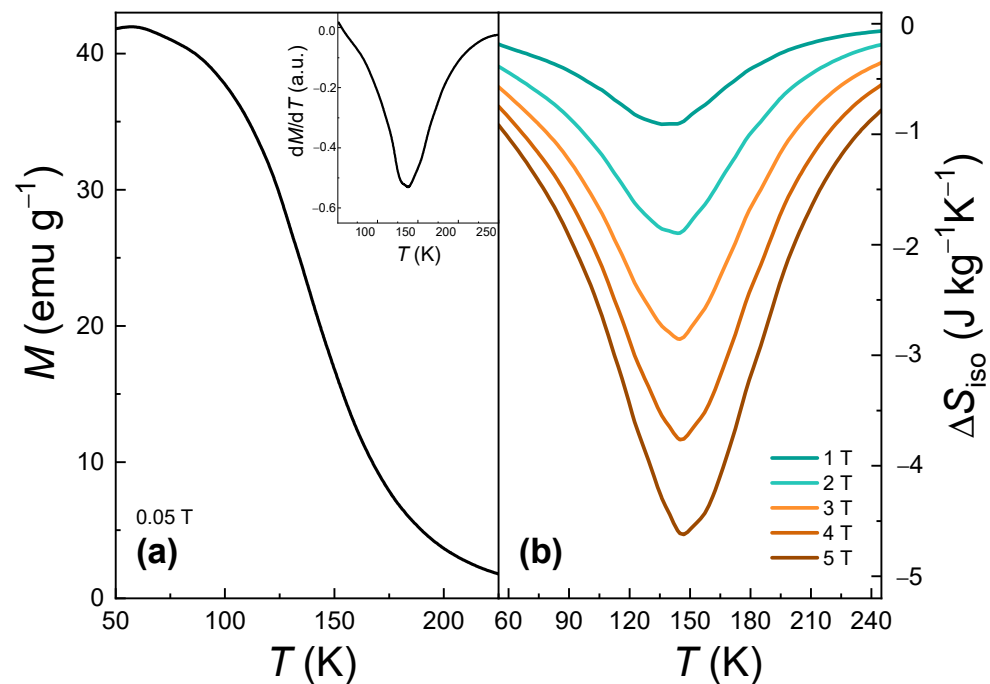


Figure 3. (a) Temperature dependence of magnetization at 0.05 T and its derivatives in the inset. (b) Isothermal magnetic entropy change as a function of temperature for the as-cast microwires for different magnetic field changes.

Figure 4a presents the XRD data and Rietveld refinement results of the studied microwires upon annealing, which shows that Fe_2P phase increases from 82.1(7) to 88.1(8) wt.%. Furthermore, the lattice parameters a shrink, and lattice parameters c expand after annealing, and the values are $a = b = 6.08589(10) \text{ \AA}$, $c = 3.45741(10) \text{ \AA}$. Figure 4b,c show the field dependence of T_{pk} and $\Delta S_{\text{iso}}^{\text{pk}}$ of the as-cast and annealed microwires. It is observed that they are enhanced upon annealing and a two-fold increase from 1.9 and 4.6 to 5.1 and 10.5 $\text{J kg}^{-1} \text{K}^{-1}$ (for a field change of 2 and 5 T) is achieved, which is comparable to Gd (9.8 $\text{J kg}^{-1} \text{K}^{-1}$ for 5 T) [27]. These larger values of $\Delta S_{\text{iso}}^{\text{pk}}$ can be attributed to the larger amount of the Fe_2P phase and to the subsequent variation in the composition (closer to the nominal one after annealing). There is slightly variation in the RCP after annealing, as shown in Figure 4d. The RCP values of microwires before and after annealing are 160 and 178 J kg^{-1} , larger than 90 J kg^{-1} of $\text{Mn}_{1.3}\text{Fe}_{0.65}\text{P}_{0.5}\text{Si}_{0.5}$ for a field change of 2 T [34], indicating a better cooling performance. The larger RCP values can be attributed to the broad ferromagnetic-paramagnetic phase transition.

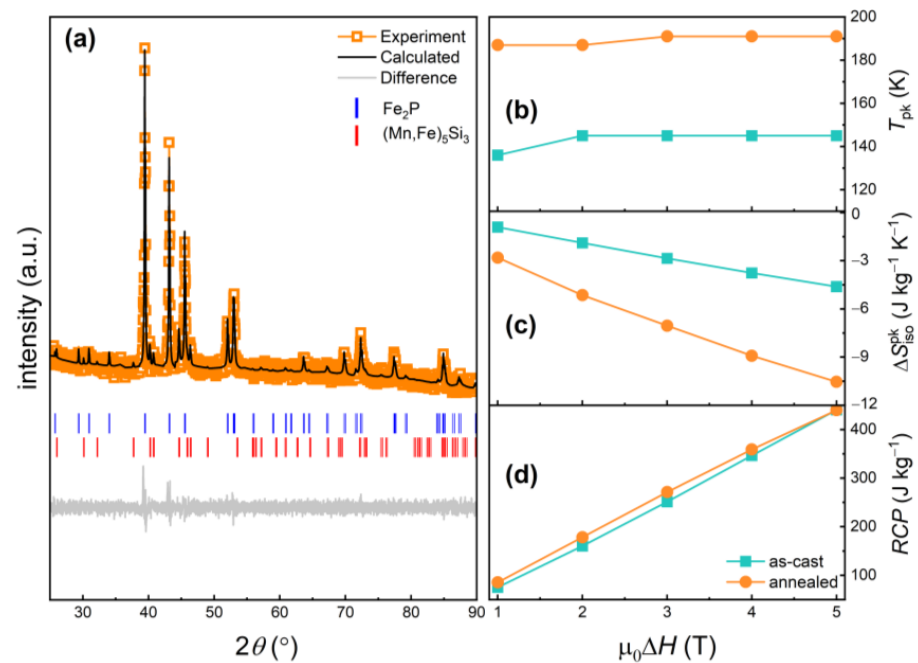


Figure 4. (a) XRD and its Rietveld refinement results; magnetic field dependence of (b) T_{pk} , (c) ΔS_{iso}^{pk} , and (d) RCP of the annealed microwires.

4. Conclusions

The $Mn_{1.3}Fe_{0.6}P_{0.5}Si_{0.5}$ microwires have been successfully fabricated by the melt-extraction technique. An elevated Fe_2P phase content of 82.1 wt.% has been attained for the as-cast microwires, which is significantly improved in comparison to conventional methods. A variable solidification structure along the radial direction of the as-cast microwires is found, from fine Fe_2P grains near the copper wheel contact \rightarrow dendritic Fe_2P grains + secondary $(Mn,Fe)_5Si_3$ phase as we advance further away from the wheel contact. The Fe_2P phase content increases up to 88.1 wt.% upon further annealing, leading to an observed two-fold increase in the isothermal magnetic entropy change peak values from 1.9 and 4.6 $J\ kg^{-1}\ K^{-1}$ to 5.1 and 10.5 $J\ kg^{-1}\ K^{-1}$ for a field change of 2 T and 5 T. The RCP values of annealed melt-extracted microwires are 178 and 440 $J\ kg^{-1}$ (for 2 T and 5 T). These results indicated that the annealed melt-extracted microwires show improved MCE performance.

Author Contributions: Conceptualization, L.L. and H.S.; methodology, L.L., J.Y.L., H.S., L.M.M.-R., S.G. and N.T.M.D.; validation, L.L., J.Y.L., H.S. and L.M.M.-R.; formal analysis, L.L. and H.S.; investigation, L.L., J.Y.L., L.M.M.-R. and H.S.; resources, J.Y.L., H.S., V.F. and J.S.; data curation, L.L.; writing—original draft preparation, L.L. and N.T.M.D.; writing—review and editing, L.L., J.Y.L., L.M.M.-R., H.S. and M.-H.P.; visualization, L.L. and J.Y.L.; supervision, V.F., J.Y.L., J.S. and M.-H.P.; project administration, V.F. and J.S.; funding acquisition, V.F. and J.S. All authors read and agree to the final version of the manuscript.

Funding: This research was funded by the National Natural Science Foundation of China (NSFC, Nos. 51871124), grant PID2019-105720RB-I00 funded by MCIN/AEI /10.13039/501100011033 and Consejería de Economía, Conocimiento, Empresas y Universidad de la Junta de Andalucía (grant P18-RT-746). L.L. acknowledges the fellowship from China Scholarship Council (CSC, 202006120203) for Visiting Ph.D. Student program. L.M.M.-R. acknowledges a postdoctoral fellowship from Junta de Andalucía and European Social Fund (ESF).

Institutional Review Board Statement: Not applicable.

Informed Consent Statement: Not applicable.

Data Availability Statement: The data presented in this study are available on request from the corresponding authors.

Conflicts of Interest: The authors declare no conflict of interest.

References

1. Franco, V.; Blázquez, J.S.; Ipus, J.J.; Law, J.Y.; Moreno-Ramírez, L.M.; Conde, A. Magnetocaloric effect: From materials research to refrigeration devices. *Prog. Mater. Sci.* **2018**, *93*, 112–232. [[CrossRef](#)]
2. Phan, M.H.; Yu, S.C. Review of the magnetocaloric effect in manganite materials. *J. Magn. Magn. Mater.* **2007**, *308*, 325–340. [[CrossRef](#)]
3. Waske, A.; Gruner, M.E.; Gottschall, T.; Gutfleisch, O. Magnetocaloric materials for refrigeration near room temperature. *Mrs Bull.* **2018**, *43*, 269–273. [[CrossRef](#)]
4. Franco, V.; Blázquez, J.S.; Ingale, B.; Conde, A. The Magnetocaloric effect and magnetic refrigeration near room temperature: Materials and models. *Annu. Rev. Mater. Res.* **2012**, *42*, 305–342. [[CrossRef](#)]
5. Kitanovski, A. Energy Applications of Magnetocaloric Materials. *Adv. Energy Mater.* **2020**, *10*, 1903741. [[CrossRef](#)]
6. Law, J.Y.; Franco, V. Pushing the limits of magnetocaloric high-entropy alloys. *APL Mater.* **2021**, *9*, 80702. [[CrossRef](#)]
7. Law, J.Y.; Franco, V. Review on magnetocaloric high-entropy alloys: Design and analysis methods. *J. Mater. Res.* **2022**, *in press*. [[CrossRef](#)]
8. Zarkevich, N.A.; Zverev, V.I. Viable materials with a giant magnetocaloric effect. *Crystals* **2020**, *10*, 815. [[CrossRef](#)]
9. Lai, J.; Tang, X.; Sepehri-Amin, H.; Hono, K. Tuning transition temperature of magnetocaloric $\text{Mn}_{1.8}\text{Fe}_{0.2}(\text{P}_{0.59}\text{Si}_{0.41})_x$ alloys for cryogenic magnetic refrigeration. *Scr. Mater.* **2020**, *183*, 127–132. [[CrossRef](#)]
10. Zhang, F.; Taake, C.; Huang, B.; You, X.; Ojiyed, H.; Shen, Q.; Dugulan, I.; Caron, L.; van Dijk, N.; Brück, E. Magnetocaloric effect in the $(\text{Mn,Fe})_2(\text{P,Si})$ system: From bulk to nano. *Acta Mater.* **2022**, *224*, 117532. [[CrossRef](#)]
11. Miao, X.F.; Hu, S.Y.; Xu, F.; Brück, E. Overview of magnetoelastic coupling in $(\text{Mn, Fe})_2(\text{P, Si})$ -type magnetocaloric materials. *Rare Metals* **2018**, *37*, 723–733. [[CrossRef](#)]
12. Lai, J.W.; Zheng, Z.G.; Huang, B.W.; Yu, H.Y.; Qiu, Z.G.; Mao, Y.L.; Zhang, S.; Xiao, F.M.; Zeng, D.C.; Goubitz, K.; et al. Microstructure formation and magnetocaloric effect of the Fe_2P -type phase in $(\text{Mn,Fe})_2(\text{P,Si,B})$ alloys. *J. Alloys Compd.* **2018**, *735*, 2567–2573. [[CrossRef](#)]
13. Zhang, F.; Batashev, I.; Shen, Q.; Wu, Z.; Smith, R.I.; de Wijs, G.A.; van Dijk, N.; Brück, E. Impact of F and S doping on $(\text{Mn,Fe})_2(\text{P,Si})$ giant magnetocaloric materials. *Acta Mater.* **2022**, *234*, 118057. [[CrossRef](#)]
14. Kim, S.; Shin, H.; Chu, I.; Lee, K.; Lee, K.H.; Lee, W. Tunable Curie temperature in $\text{Mn}_{1.15}\text{Fe}_{0.85}\text{P}_{0.55}\text{Si}_{0.45}$ via lattice engineering by Al addition. *J. Alloys Compd.* **2022**, *890*, 161798. [[CrossRef](#)]
15. Zheng, Z.G.; Tan, Z.C.; Yu, H.Y.; Zhang, J.L.; Zeng, D.C.; Franco, V. Structural, magnetic properties and magnetocaloric effect of $\text{Mn}_{1.2}\text{Fe}_{0.8}\text{P}_{1-x}\text{Si}_xB_{0.03}$ compounds. *Mater. Res. Bull.* **2016**, *77*, 29–34. [[CrossRef](#)]
16. Zheng, Z.G.; Wang, W.H.; Zhou, Q.; Lei, L.; Hong, Y.; Zeng, D.C.; Mozharivskiy, Y. Microstructure and magnetocaloric effects of $\text{Mn}_{1.2}\text{Fe}_{0.8}\text{P}_{0.6}\text{Si}_{0.4}\text{B}_{0.05}$ alloys prepared by ball milling and spinning methods. *J. Magn. Magn. Mater.* **2019**, *477*, 203–208. [[CrossRef](#)]
17. Tu, D.; Li, J.; Zhang, R.; Hu, Q.; Li, J. Microstructure evolution, solidification characteristic and magnetocaloric properties of $\text{MnFeP}_{0.5}\text{Si}_{0.5}$ particles by droplet melting. *Intermetallics* **2021**, *131*, 107102. [[CrossRef](#)]
18. Tu, D.; Li, J.; Dong, Z.; Zeng, L.; Xia, M.; Hu, Q.; Li, J. Effect of heat treatment on microstructure evolution and magnetocaloric properties of droplet melted Mn-Fe-P-Si alloys. *J. Mater. Res. Technol.* **2022**, *20*, 1593–1602. [[CrossRef](#)]
19. Shen, H.; Wang, H.; Liu, J.; Xing, D.; Qin, F.; Cao, F.; Chen, D.; Liu, Y.; Sun, J. Enhanced magnetocaloric and mechanical properties of melt-extracted $\text{Gd}_{55}\text{Al}_{25}\text{Co}_{20}$ micro-fibers. *J. Alloys Compd.* **2014**, *603*, 167–171. [[CrossRef](#)]
20. Qin, F.X.; Bingham, N.S.; Wang, H.; Peng, H.X.; Sun, J.F.; Franco, V.; Yu, S.C.; Srikanth, H.; Phan, M.H. Mechanical and magnetocaloric properties of Gd-based amorphous microwires fabricated by melt-extraction. *Acta Mater.* **2013**, *61*, 1284–1293. [[CrossRef](#)]
21. Yin, H.; Law, J.Y.; Huang, Y.; Shen, H.; Jiang, S.; Guo, S.; Franco, V.; Sun, J. Enhancing the magnetocaloric response of high-entropy metallic-glass by microstructural control. *Sci. China Mater.* **2022**, *65*, 1134–1142. [[CrossRef](#)]
22. Yin, H.; Law, J.; Huang, Y.; Franco, V.; Shen, H.; Jiang, S.; Bao, Y.; Sun, J. Design of Fe-containing GdTbCoAl high-entropy-metallic-glass composite microwires with tunable Curie temperatures and enhanced cooling efficiency. *Mater. Des.* **2021**, *206*, 109824. [[CrossRef](#)]
23. Shen, H.; Luo, L.; Bao, Y.; Yin, H.; Jiang, S.; Zhang, L.; Huang, Y.; Feng, S.; Xing, D.; Liu, J.; et al. New DyHoCo medium entropy amorphous microwires of large magnetic entropy change. *J. Alloys Compd.* **2020**, *837*, 155431. [[CrossRef](#)]
24. Vuarnoz, D.; Kawanami, T. Numerical analysis of a reciprocating active magnetic regenerator made of gadolinium wires. *Appl. Therm. Eng.* **2012**, *37*, 388–395. [[CrossRef](#)]
25. Kuz'Min, M.D. Factors limiting the operation frequency of magnetic refrigerators. *Appl. Phys. Lett.* **2007**, *90*, 251916. [[CrossRef](#)]
26. He, A.; Mozharivskiy, Y. Structural and magnetic properties of the $\text{MnFeSi}_x\text{P}_{1-x}$ magnetocaloric phases. *Intermetallics* **2019**, *105*, 56–60. [[CrossRef](#)]

27. He, A.; Svitlyk, V.; Mozharivskyj, Y. Synthetic Approach for $(\text{Mn,Fe})_2(\text{Si,P})$ Magnetocaloric Materials: Purity, Structural, Magnetic, and Magnetocaloric Properties. *Inorg. Chem.* **2017**, *56*, 2827–2833. [[CrossRef](#)]
28. Pęczkowski, P.; Zachariasz, P.; Kowalik, M.; Tokarz, W.; Naik, S.P.K.; Żukrowski, J.; Jastrzębski, C.; Dadiel, L.J.; Tabiś, W.; Gondek, A. Iron diffusivity into superconducting $\text{YBa}_2\text{Cu}_3\text{O}_{7-\delta}$ at oxygen-assisted sintering: Structural, magnetic, and transport properties. *J. Eur. Ceram. Soc.* **2021**, *41*, 7085–7097. [[CrossRef](#)]
29. Li, C.F.; Zheng, Z.G.; Wang, W.H.; Liu, J.Y.; Lei, L.; Zeng, D.C. Effect of M/NM ratios on structural and magnetic properties of $(\text{Mn,Fe})_2(\text{P,Si})$ compounds. *Phys. B Condens. Matter* **2020**, *594*, 412309. [[CrossRef](#)]
30. Grebenkemper, J.H.; Bocarsly, J.D.; Levin, E.E.; Seward, G.; Heikes, C.; Brown, C.; Misra, S.; Seeler, F.; Schierle-Arndt, K.; Wilson, S.D.; et al. Rapid Microwave Preparation and Composition Tuning of the High-Performance Magnetocalorics $(\text{Mn,Fe})_2(\text{P,Si})$. *ACS Appl. Mater. Inter.* **2018**, *10*, 7208–7213. [[CrossRef](#)]
31. Franco, V. Determination of the Magnetic Entropy Change from Magnetic Measurements: The Importance of the Measurement Protocol. Available online: http://www.lakeshore.com/docs/default-source/software/vsm/mce-software/determination-of-the-magnetic-entropy-change-from-magnetic-measurements.pdf?sfvrsn=d14f68c1_2 (accessed on 16 September 2014).
32. Zheng, Z.; Wang, H.; Li, C.; Chen, X.; Zeng, D.; Yuan, S. Enhancement of Magnetic Properties and Magnetocaloric Effects for $\text{Mn}_{0.975}\text{Fe}_{0.975}\text{P}_{0.5}\text{Si}_{0.5}$ Alloys by Optimizing Quenching Temperature. *Adv. Eng. Mater.* **2022**, *2022*, 2200160. [[CrossRef](#)]
33. Pęczkowski, P.; Buszczek, M.; Szostak, E.; Muniraju, N.K.C.; Krztoń-Maziopa, A.; Gondek, A. Superconductivity and appearance of negative magnetocaloric effect in $\text{Ba}_{1-x}\text{K}_x\text{BiO}_3$ perovskites, doped by Y, La and Pr. *Acta Mater.* **2022**, *222*, 117437. [[CrossRef](#)]
34. Habiba, U.E.; Khattak, K.S.; Ali, S.; Khan, Z.H. MnAs and $\text{MnFeP}_{1-x}\text{As}_x$ -based magnetic refrigerants: A review. *Mater. Res. Express* **2020**, *7*, 46106. [[CrossRef](#)]